Frequency-domain tools for stability analysis of reset control systems

S.J.L.M. van Loon, K.G.J. Gruntjens, M.F. Heertjes, N. van de Wouw**, W.P.M.H. Heemels

Eindhoven University of Technology, Dep. of Mechanical Engineering, P.O. Box 513, NL 5600 MB Eindhoven, the Netherlands.

Abstract

The potential of reset controllers to improve the transient performance of linear (motion) systems has been extensively demonstrated in the literature. The design and stability analysis of these reset controllers generally rely on the availability of parametric models and on the numerical solution of linear matrix inequalities. Both these aspects may hamper the application of reset control in industrial settings. To remove these hurdles and stimulate broader application of reset control techniques in practice, we present new sufficient conditions, based on measured frequency response data of the system to be controlled, to guarantee the stability of closed-loop reset control systems. The effectiveness of these conditions is demonstrated through experiments on an industrial piezo-actuated motion system.

Key words: Reset control; Frequency-domain methods; Circle criterion; Input-to-state stability

1 Introduction

A reset controller is a linear time-invariant (LTI) control system of which the state, or a part of the state is reset to a certain value (usually zero) whenever appropriate algebraic conditions on its input and output are satisfied. Reset controllers were proposed in 1958, see [10], in order to overcome the inherent performance limitations of linear feedback controllers imposed by Bode's gain-phase relationship. Especially in the last two decades, reset control has regained attention from the control community in both theoretically oriented research, see e.g., [1, 2, 4, 5, 19, 20, 22, 30], as well as in applications [2, 13, 21, 31]. However, despite the potential of a reset controller to improve the transient performance of linear systems, reset controllers are often not so easily embraced by (motion) control engineers in industry. To a large extent, this is caused by the fact that the vast majority of existing tools for the stability analysis and the design of reset controllers rely on parametric models and on solving linear matrix inequalities using those models. As such, they do not interface well with the current industrial (motion) control design practice, in which typically frequency-domain tools and non-parametric models are exploited, see, e.g., [7]. Therefore, an important open problem is to obtain easy-to-use, 'industry-friendly' design tools for reset control systems using frequency-domain techniques as a basis.

In this paper, we contribute to solving this important open problem and focus, in particular, on deriving stability conditions that are graphically verifiable on the basis of *measured* frequency response data concerning the system dynamics. These conditions apply, amongst others, to the reset condition employed in [1,11,20,29], and have some connections to recent developments in variable gain control (VGC), see, e.g., [14, 17, 27]. In VGC, the use of the circle criterion, see, e.g., [18], is central in obtaining stability conditions based on frequency-domain system models. A key step in the approach for VGC is to write the closed-loop system as a so-called Lur'e-type system, i.e., a feedback interconnection of an LTI dynamical system and a static memoryless nonlinearity, see [18]. Un-

⋆ This research is financially supported by the Dutch Technology Foundation (STW) under the projects "HyperMotion: Hybrid control for performance improvement of linear motion systems" (no. 10953) and CHAMELEON: "Hybrid solutions for cost-aware high-performance motion control" (no. 13896).

⋆⋆N. van de Wouw is also with the Department of Civil, Environmental and Geo-Engineering, University of Minnesota, Minneapolis, MN 55455 USA, and with the Delft Center for Systems and Control, Delft University of Technology, Delft, The Netherlands.

⋆⋆⋆E-mail addresses: {s.j.l.m.v.loon, k.g.j.gruntjens, m.f.heertjes, n.v.d.wouw, m.heemels}@tue.nl

fortunately, such an approach does not transfer easily to reset controllers as the closed-loop system would be an interconnection of an LTI dynamical system and a reset controller. This is not a (true) Lur'e-type system as the reset controller (as opposed to the VGC element) consists of a *dynamical* system that exhibits discontinuities (jumps) in the state variables rather than a static memoryless element. As such, applying Lur'e-type stability arguments calls for a new perspective on reset control systems, which we will provide in this paper by abstracting away from the internal dynamics of the reset controller and focusing instead on its input/output behavior, that can be confined to a certain sector bound, see [18]. This sector bound can subsequently be employed in a circle criterion-like condition. We will formally prove that this will yield sufficient conditions to assess input-to-state stability (ISS), see [8, 25], of reset control systems (including the internal dynamics) by evaluating (measured) frequency response data. In addition, this new perspective on reset control can also be directly used for the design of such controllers.

The results presented in this paper are not the first stability conditions for reset control systems that are graphically verifiable on the basis of *measured* frequency response data. In [6], see also [4] containing an overview of the work on reset control until the mid 2000s, the H_β-condition was developed involving a strictly positive real condition to guarantee closed-loop stability of a class of reset control systems. However, the result still required a parametric model for the search of both a positive definite matrix and a vector (both of size equal to the dimension of the states of the controller that are reset) defining the output of the transfer matrix that has to be strictly positive real. In this paper, we aim for frequency-domain conditions for the analysis and design of reset control systems, i.e., employing measured data instead of using parametric models, with the additional advantage that the linear part of the controller design and analysis can be performed by shaping the frequency response of the open-loop and/or closed-loop transfer functions, see [26]. In [9,11], the concept of passivity has been used to analyze stability of reset systems. Key in the work of [9] is that a (full) reset system retains the passivity properties of its underlying base system, i.e., the system without the reset part. As a result, $\mathcal{L}_2$-stability conditions can be verified in the frequency domain. In addition, the results in [11] can be seen as a generalization of the results in [9]. The novelty in our stability results compared to [9, 11] is the link to the circle criterion, resulting in less strict conditions on the underlying base system. The relaxation lies in the fact that the underlying linear system does not need to be strictly positive real (as in [9,11]) but should satisfy less stringent (circle-criterion) conditions. This fact significantly widens the applicability scope of the results. An important class of systems for which such relaxation is essential for the application of reset control, is the class of motion control systems as studied as a central application in this paper.

The outline of this paper is as follows. In Section 2, we present the control architecture. In Section 3, we present our main results. In Section 4, we discuss an industrial case study and demonstrate the applicability of the presented results in practice. Finally in Section 5, we provide the conclusions.

1.1 Nomenclature

The following notational conventions will be used. Let $\mathbb{N}$, $\mathbb{R}$, $\mathbb{R}_{\geq 0}$, $\mathbb{C}$ denote the set of non-negative integers, real numbers, nonnegative real numbers and complex numbers, respectively. The Laplace transform of a signal $x : \mathbb{R}_{\geq 0} \to \mathbb{R}^n$ is denoted by $\mathfrak{L}\{x\}$ and $s \in \mathbb{C}$ denotes the Laplace variable. Some further hybrid system notations from [12] can be found in Appendix A.

2 System description and problem formulation

In this section, we will formally introduce the reset control system as considered in this paper and derive a closed-loop hybrid model. In addition, we pose a problem formulation.

2.1 Hybrid closed-loop model

We will mainly focus on the single-input-single-output (SISO) control architecture as depicted in Fig. 1, although our results are applicable to other configurations as well, see Remark 8 below. The closed-loop system in Fig. 1 consists of a linear time-invariant (LTI) plant given by the transfer function $\mathcal{P}(s)$, $s \in \mathbb{C}$, a nominal LTI controller with transfer function $\mathcal{C}(s)$, reference $r \in \mathbb{R}$, output $y_p \in \mathbb{R}$, tracking error $e := r - y_p \in \mathbb{R}$ and an external disturbance $d \in \mathbb{R}$. In this figure, $\mathcal{R}$ denotes a reset controller, which is modeled in terms of the hybrid system formalism of [12] as

$$\mathcal{R} : \begin{cases} \dot{x}_r = A_r x_r + B_r e & \text{if } (e, -u) \in \mathcal{F} \\ x_r^+ = 0 & \text{if } (e, -u) \in \mathcal{J} \\ u = -C_r x_r \end{cases} \tag{1}$$

with state $x_r \in \mathbb{R}^{n_r}$, controller output $u \in \mathbb{R}$, and A_r, B_r, C_r are constant real matrices of appropriate dimensions. In (1), flow of the reset controller state x_r occurs when the input/output pair $(e, -u)$ is in the flow set $\mathcal{F}$ given by

$$\mathcal{F} := \{(e, -u) \in \mathbb{R}^2 \,|\, eu \leq -\tfrac{1}{\alpha} u^2\} \tag{2a}$$

with $\alpha \in (0, \infty)$, and state resets occur when the input/output pair $(e, -u)$ is in the jump set $\mathcal{J}$ given by

$$\mathcal{J} := \{(e, -u) \in \mathbb{R}^2 \,|\, eu \geq -\tfrac{1}{\alpha} u^2\}. \tag{2b}$$

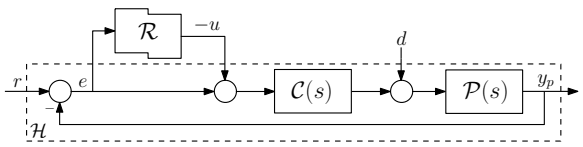

Fig. 1. Schematic representation of a reset control scheme.

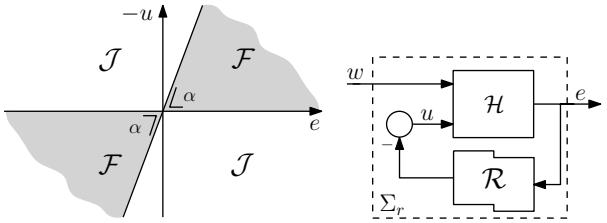

Fig. 2. (a) Schematic representation of the flow set $\mathcal{F}$ and jump set $\mathcal{J}$, (b) Feedback interconnection between an LTI dynamical system $\mathcal{H}$ as in (5) and $\mathcal{R}$ as in (1), (2).

A schematic representation of the flow set $\mathcal{F}$ and the jump set $\mathcal{J}$ can be found in Fig. 2(a). Later, the concept of hybrid time domains and solutions (solution pairs) of hybrid systems of the form (1), (2) will be used, which are defined for a general class of hybrid systems with inputs in Appendix A for convenience of the reader. For more details on this hybrid modeling framework we refer the reader to [8, 12].

Remark 1 *The general class of reset controllers in* (1), (2) *encompasses two of the most well-known reset controllers in the literature, i.e., the Clegg integrator [10] and the First-Order-Reset-Element (FORE) [16]. Indeed, these can be can be modeled as in* (1) *using*

$$\textit{Clegg integrator}: \ (A_r, B_r, C_r) = (0, \omega_i, 1), \tag{3}$$
$$\textit{FORE}: \ (A_r, B_r, C_r) = (\beta, \omega_i, 1), \tag{4}$$

in which $n_r = 1$, $\omega_i \in \mathbb{R}_{\geq 0}$ *represents the integrator gain, and* $\beta \in \mathbb{R}$ *denotes the single pole of the FORE, see, e.g., [28] and the references therein.*

Let us adopt the following assumption on the reset controller (1), (2).

Assumption 2 *The pair* (A_r, C_r) *is detectable.*

Remark 3 *Note that Assumption 2 is trivially satisfied for the Clegg integrator and the FORE because they are both one-dimensional systems* ($n_r = 1$) *and* $C_r \neq 0$.

The closed-loop system in Fig. 1 can be written as a feedback interconnection between an LTI dynamical system $\mathcal{H}$ and the reset controller $\mathcal{R}$, as depicted in Fig. 2(b). In Fig. 2(b), the LTI dynamical system $\mathcal{H}$ is given by

$$\mathcal{H}: \begin{cases} \dot{\xi} = A\xi + Bu + B_w w & \text{(5a)} \\ e = C\xi + D_w w & \text{(5b)} \end{cases}$$

with state $\xi \in \mathbb{R}^{n_\xi}$ containing the states of both the plant $\mathcal{P}(s)$ as well as those of the nominal LTI controller $\mathcal{C}(s)$, and the external inputs are denoted by $w = [r \ \ d]^\top \in \mathbb{R}^2$. Moreover, it is assumed that (A, B, C) is minimal such that

$$\mathfrak{L}\{e\} = \mathcal{G}_{eu}(s)\mathfrak{L}\{u\} + \mathcal{G}_{ew}(s)\mathfrak{L}\{w\}, \tag{6}$$

in which the transfer function between 'input' u and 'output' e, see Fig. 2(b), is given by

$$\mathcal{G}_{eu}(s) = C(sI - A)^{-1}B = \frac{\mathcal{P}(s)\mathcal{C}(s)}{1 + \mathcal{P}(s)\mathcal{C}(s)}, \tag{7}$$

and the transfer function between the external inputs w and e is given by

$$\begin{aligned} \mathcal{G}_{ew}(s) &= C(sI - A)^{-1}B_w + D_w \\ &= \begin{bmatrix} \frac{1}{1+\mathcal{P}(s)\mathcal{C}(s)} & \frac{-\mathcal{P}(s)}{1+\mathcal{P}(s)\mathcal{C}(s)} \end{bmatrix}. \end{aligned} \tag{8}$$

The closed-loop system in Fig. 2(b) with $\mathcal{H}$ as in (5), and $\mathcal{R}$ as in (1), (2), can be written as the hybrid model

$$\Sigma_r: \begin{cases} \dot{x} = \bar{A}x + \bar{B}w, & \text{if } (e, -u) \in \mathcal{F}, & \text{(9a)} \\ x^+ = \bar{A}_r x, & \text{if } (e, -u) \in \mathcal{J}, & \text{(9b)} \\ u = -\bar{C}_r x & & \text{(9c)} \\ e = \bar{C}x + D_w w & & \text{(9d)} \end{cases}$$

with augmented state vector $x := [\xi^\top \ x_r^\top]^\top \in \mathbb{R}^{n_x}$, $n_x = n_\xi + n_r$, and

$$\bar{A} = \begin{bmatrix} A & -BC_r \\ B_r C & A_r \end{bmatrix}, \ \bar{B} = \begin{bmatrix} B_w \\ B_r D_w \end{bmatrix}, \ \bar{A}_r = \begin{bmatrix} I_{n_\xi} & 0 \\ 0 & 0 \end{bmatrix},$$
$$\bar{C}_r = \begin{bmatrix} 0 & C_r \end{bmatrix}, \text{ and } \bar{C} = \begin{bmatrix} C & 0 \end{bmatrix}. \tag{9e}$$

2.2 Problem formulation

The objective of this paper is to derive sufficient conditions to assess (input-to-state) stability of the hybrid system (9) with (2), based on (measured) frequency response data of the linear part $\mathcal{G}_{eu}(j\omega)$, $\omega \in \mathbb{R}$, of the closed-loop system dynamics.

Definition 4 *The closed-loop hybrid system* Σ_r *as in* (9) *with* (2)*, is said to be pre-input-to-state stable (pre-ISS), if there exist a* $\mathcal{KL}$*-function* β *and* $\mathcal{K}$*-function* γ *such that for any solution pair* (x, w) *to* (9), (2) *with* $w \in \mathcal{L}_\infty$ *it holds that*

$$\|x(t, j)\| \leq \beta(\|x(0, 0)\|, t) + \gamma\left(\|w\|_\infty\right) \tag{10}$$

for all $(t, j) \in \mathit{dom}\, x$.

Remark 5 *Our definition of pre-ISS differs from the definition of ISS for hybrid systems as in [8]. First, we are primarily interested in the evolution of the state x over continuous time t, and less in the number of 'resets/jumps' the solution has experienced, see [8, 12]. Second, in line with the notions of pre-attractivity and pre-asymptotic stability in [12], we adopt here pre-ISS (as opposed to ISS) to indicate the possibility of maximal solutions not being complete (e.g., not having solutions with domains that are unbounded in the t-direction). As argued in [12, Sec. 3.1], allowing this phenomenon separates conditions for completeness of solutions (having unbounded hybrid time-domains), which is related to questions on global existence of solutions (see [3] for a recent study) from conditions for stability and ISS. In this paper, existence and t-completeness of solutions are implicitly assumed. For closed-loop reset control systems in which this is not satisfied, a good solution is the inclusion of temporal regularization, see, e.g., [11, 20, 29], in* (1), (2) *in which a positive minimal time is enforced between two resets and existence and t-completeness will follow from pre-ISS and will result in standard ISS. Including time regularization is beyond the scope of the current paper and is a topic of future work, which can be based on the new idea in this paper that leads to novel frequency-domain conditions. Moreover, the fact that any practical digital implementation of the proposed control strategy employs sampling and hold mechanisms could also lead to resolving the absence of t-completeness. This is further supported by the experimental results presented in Section 4. In any case, the results in this paper guarantee the property* (10) *for any t-complete solution.*

3 Frequency-domain tools for stability analysis

In this section, we present our main result in the form of a theorem consisting of novel data-based conditions guaranteeing pre-ISS for reset control systems described by (9) with (2).

Theorem 6 *Consider the hybrid system Σ_r as in* (9) *with* (2) *and fixed $\alpha \in (0, \infty)$, and let Assumption 2 hold. Then, Σ_r is pre-ISS according to Definition 4 if the following conditions are satisfied:*

(I) The system matrix A of (5) *is Hurwitz;*
(II) The transfer function $\mathcal{G}_{eu}(s)$ as in (8) *satisfies*

$$\tfrac{1}{\alpha} + Re(\lim_{\omega \to \infty} \mathcal{G}_{eu}(j\omega)) > 0 \tag{11}$$

and

$$\tfrac{1}{\alpha} + Re(\mathcal{G}_{eu}(j\omega)) > 0 \quad \textit{for all } \omega \in \mathbb{R}. \tag{12}$$

PROOF. The proof is based on constructing an ISS Lyapunov (ISSLF), see [8], for the hybrid system Σ_r, which is a smooth function $W : \mathbb{R}^{n_x} \to \mathbb{R}$ satisfying, for $\kappa_i > 0$, $i = 1, 2, 3, 4$, the following conditions

$$\kappa_1 \|x\|^2 \leq W(x) \leq \kappa_2 \|x\|^2 \tag{13a}$$
$$\dot{W}(x) \leq -\kappa_3 \|x\|^2 + \kappa_4 \|w\|^2 \quad \text{when } (e, -u) \in \mathcal{F} \tag{13b}$$
$$W(x^+) \leq W(x) \qquad \text{when } (e, -u) \in \mathcal{J}. \tag{13c}$$

We do this following four steps:

- Step 1: We disregard the internal dynamics of $\mathcal{R}$ and exploit the fact that the input/output pairs $(e, -u)$ of $\mathcal{R}$ satisfy the sector condition $eu \leq -\frac{1}{\alpha}u^2$ by the grace of the form of $\mathcal{F}$ and $\mathcal{J}$ in (2). Moreover, note that the hypothesis of the theorem imply strict positive realness of the transfer function

$$\tilde{\mathcal{G}}_{eu}(s) := \mathcal{G}_{eu}(s) + \tfrac{1}{\alpha} = C(sI - A)^{-1}B + \tfrac{1}{\alpha}. \tag{14}$$

  This knowledge will be combined with a circle criterion reasoning to prove that the system (5) together with the sector condition $eu \leq -\frac{1}{\alpha}u^2$ admits an ISS Lyapunov function (ISSLF) $V : \mathbb{R}^{n_\xi} \to \mathbb{R}$, see [25];
- Step 2: We show that the detectability condition in Assumption 2 can be converted to a Lyapunov-like function $V_r : \mathbb{R}^{n_r} \to \mathbb{R}$;
- Step 3: We show that the functions V of Step 1 and V_r of Step 2 can be combined into a function $W : \mathbb{R}^{n_x} \to \mathbb{R}$, and that we satisfy condition (13b) during flow;
- Step 4: We show that the ISSLF constructed in Step 3 does not increase during resets, thereby also satisfying the ISSLF condition during jumps, i.e., (13c). This allows us to construct a bound on the norm of the total state as in (10).

Step 1: Using the Kalman-Yakubovich-Popov lemma, see [18], under hypothesis (I) and (II) of the theorem and minimality of (A, B, C) (and thus strict positive realness of (14)), there exist matrices L, H, $P = P^\top \succ 0$, and a positive constant ε such that

$$A^\top P + PA = -L^\top L - \varepsilon P \tag{15a}$$
$$PB = C^\top - \sqrt{\tfrac{2}{\alpha}} L^\top \tag{15b}$$
$$H^\top H = \tfrac{2}{\alpha}. \tag{15c}$$

Let us take $V(\xi) = \frac{1}{2}\xi^\top P \xi$ as a candidate ISSLF, satisfying

$$\lambda_{min}(P)\|\xi\|^2 \leq V(\xi) \leq \lambda_{max}(P)\|\xi\|^2, \tag{16}$$

in which $\lambda_{min}(P)$ and $\lambda_{max}(P)$ denote the minimum and the maximum eigenvalue of P, respectively, and for

which the time derivative along solutions of (5) satisfies

$$\begin{aligned}\dot{V} &= \tfrac{1}{2}\xi^\top(A^\top P + PA)\xi + \xi^\top PBu + \xi^\top PB_w w \\ &\overset{(15)}{=} -\tfrac{\varepsilon}{2}V - \tfrac{1}{2}\xi^\top L^\top L\xi + \xi^\top\left(C^\top - L^\top\sqrt{\tfrac{2}{\alpha}}\right)u + \\ &\qquad \xi^\top PB_w w \\ &\overset{(5b)}{=} -\tfrac{\varepsilon}{2}V - \tfrac{1}{2}\xi^\top L^\top L\xi - \sqrt{\tfrac{2}{\alpha}}\xi^\top L^\top u + eu + \\ &\qquad \left(\xi^\top PB_w - uD_w\right)w \\ &\leq -\tfrac{\varepsilon}{2}V - \tfrac{1}{2}\xi^\top L^\top L\xi - \sqrt{\tfrac{2}{\alpha}}\xi^\top L^\top u - \tfrac{1}{\alpha}u^2 + \\ &\qquad \left(\xi^\top PB_w - uD_w\right)w \\ &= -\tfrac{\varepsilon}{2}V - \tfrac{1}{2}\left(L\xi + \sqrt{\tfrac{2}{\alpha}}u\right)^\top\left(L\xi + \sqrt{\tfrac{2}{\alpha}}u\right) + \\ &\qquad \left(\xi^\top PB_w - uD_w\right)w \\ &\leq -\tfrac{\varepsilon}{2}V + \left(\xi^\top PB_w - uD_w\right)w \end{aligned} \tag{17}$$

in which we have used the sector condition, i.e., $eu \leq -\frac{1}{\alpha}u^2$. Moreover, note that

$$\begin{aligned}&\left(\xi^\top PB_w - uD_w\right)w \\ &\quad\leq \lambda_{max}(P)\|B_w\|\|w\|\|\xi\| + \|D_w\|\|u\|\|w\| \\ &\quad\leq \lambda_{max}(P)\|B_w\|\|w\|\|\xi\| + \alpha\|D_w\|\|C\xi + D_w w\|\|w\| \\ &\quad\leq c_1\|w\|\|\xi\| + c_2\|w\|^2 \\ &\quad\leq \tfrac{1}{\delta_1}\|\xi\|^2 + (c_1^2\delta_1 + c_2)\|w\|^2, \end{aligned} \tag{18}$$

for any $\delta_1 > 0$, in which $c_1 := (\lambda_{max}(P)\|B_w\| + \alpha\|D_w\|\|C\|) > 0$ and $c_2 := \alpha\|D_w\|^2 > 0$. Note that we explicitly used $\|u\| \leq \alpha\|e\|$ and (5b) in the second inequality. Using (18) in (17) yields

$$\dot{V} \leq -c_3\|\xi\|^2 + c_4\|w\|^2 \tag{19}$$

with $c_3 := \left(\frac{\varepsilon\lambda_{min}(P)}{2} - \frac{1}{\delta_1}\right)$ and $c_4 := (c_1^2\delta_1 + c_2)$. Note that c_3 and c_4 are both positive if δ_1 is taken sufficiently large.

Step 2: Assumption 2 implies that there exists a matrix K such that $A_r + KC_r$ is Hurwitz, see, e.g., [15]. Consequently, there exists a $P_r = P_r^\top \succ 0$ such that the following Lyapunov equality holds

$$(A_r + KC_r)^\top P_r + P_r(A_r + KC_r) = -I. \tag{20}$$

Let us take $V_r(x_r) = x_r^\top P_r x_r$ as a Lyapunov-like function for the system (1) with input e during flow, satisfying for all $x_r \in \mathbb{R}^{n_r}$

$$\lambda_{min}(P_r)\|x_r\|^2 \leq V_r(x_r) \leq \lambda_{max}(P_r)\|x_r\|^2. \tag{21}$$

The time-derivative of V_r along the flow dynamics of $\mathcal{R}$ in (1) satisfies

$$\dot{V}_r = x_r^\top\left(A_r^\top P_r + P_r A_r\right)x_r + 2x_r^\top P_r B_r e. \tag{22}$$

Note that (20) implies

$$\begin{aligned}x_r^\top\left(A_r^\top P_r + P_r A_r\right)x_r &= -\|x_r\|^2 - 2x_r^\top C_r^\top K^\top P_r x_r \\ &= -\|x_r\|^2 + 2u^\top K^\top P_r x_r \\ &\leq -c_5\|x_r\|^2 + c_6\|u\|^2 \end{aligned} \tag{23}$$

with $c_5 := (1 - \frac{1}{\delta_2}) > 0$, $c_6 := (2\lambda_{max}(P_r)\|K\|)^2\delta_2 > 0$ for $\delta_2 > 1$. Using (23) in (22) yields

$$\begin{aligned}\dot{V}_r &\leq -c_5\|x_r\|^2 + c_6\|u\|^2 + 2x_r^\top P_r B_r e \\ &\leq -c_7\|x_r\|^2 + c_6\|u\|^2 + c_8\|e\|^2 \end{aligned} \tag{24}$$

with $c_7 := (c_5 - \frac{1}{\delta_3}) > 0$, $c_8 := (2\lambda_{max}(P_r)\|B_r\|)^2\delta_3 > 0$ for $\delta_3 > 0$. Using again $\|u\| \leq \alpha\|e\|$, this yields

$$\begin{aligned}\dot{V}_r &\leq -c_7\|x_r\|^2 + c_9\|e\|^2 \\ &\overset{(5b)}{\leq} -c_7\|x_r\|^2 + c_{10}\|\xi\|^2 + c_{11}\|w\|^2 \end{aligned} \tag{25}$$

with $c_9 =: (\alpha^2 c_6 + c_7^2\delta_3) > 0$, $c_{10} := c_9(\|C\|^2 + \frac{1}{\delta_4}) > 0$ and $c_{11} := c_9(4\delta_4\|C\|^2\|D_w\|^2 + \|D_w\|^2) > 0$ for $\delta_4 > 0$.

Step 3: Let us construct the following candidate ISSLF

$$W(\xi, x_r) = V(\xi) + \mu V_r(x_r) = x^\top P_w x, \tag{26}$$

for some $\mu > 0$ and $P_w = \mathrm{diag}(P, \mu P_r)$, satisfying (13a) with $\kappa_1 = \lambda_{min}(P_w)$ and $\kappa_2 = \lambda_{max}(P_w)$. The time-derivative of W along flow of (9), (2) satisfies

$$\begin{aligned}\dot{W} &= \dot{V} + \mu\dot{V}_r \\ &\leq -(c_3 - \mu c_{10})\|\xi\|^2 - \mu c_7\|x_r\|^2 + (c_4 + \mu c_{11})\|w\|^2 \\ &\leq -\kappa_3\|x\|^2 + \kappa_4\|w\|^2 \end{aligned} \tag{27}$$

with $\kappa_3 := \min((c_3 - \mu c_{10}), \mu c_7)$, $\kappa_4 := c_4 + \mu c_{11}$, and for sufficiently small μ such that $(c_3 - \mu c_{10}) > 0$. Hence, W satisfies (13b).

Step 4: Due to (1) the function W constructed in *Step 3* satisfies

$$W(\xi^+, 0) \leq W(\xi, x_r) \tag{28}$$

during jumps of (9), (2). Consequently, for a solution pair (x, w) to (9), (2), with input disturbance $w \in \mathcal{L}_\infty$, we obtain from (13a), (27) and (28), and using similar arguments as in [8, 25], for $(t, j) \in \mathrm{dom}\, x$ that

$$\dot{W} \leq -\sigma_1 W \quad \text{when } \|x\| \geq \sigma_2\|w\| \tag{29}$$

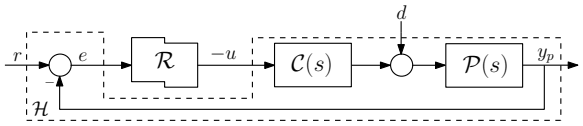

Fig. 3. Schematic representation of a reset control scheme.

with $\sigma_1 := \frac{\kappa_3}{2\kappa_2}$ and $\sigma_2 := \sqrt{\frac{2\kappa_4}{\kappa_3}}$. Consequently, for all $(t, j) \in \operatorname{dom} x$ we have

$$\|x(t,j)\| \leq \sqrt{\tfrac{\kappa_2}{\kappa_1}} e^{-\frac{\sigma_1}{2}t} \|x(0,0)\| + \sqrt{\tfrac{\kappa_2}{\kappa_1}} \sigma_2 \|w\|_\infty. \quad (30)$$

The latter inequality shows that the system (9), (2) is pre-ISS according to Definition 4. This completes the proof. □

Remark 7 *Considering the conditions in Theorem 6, the following remarks are in order:*

(1) Condition (I) will be satisfied by the design of a stabilizing feedback controller $\mathcal{C}(s)$, i.e., an LTI controller designed to stabilize the LTI plant $\mathcal{P}(s)$. This is due to the fact that if the open-loop $\mathcal{P}(s)\mathcal{C}(s)$ satisfies the Nyquist stability criterion, see, e.g., [24], $\mathcal{G}_{eu}(s)$ as in (8) *(which represents the complementary sensitivity function) has all its poles located in the complex left half plane (LHP) and the system matrix A of* (5) *will be Hurwitz (under minimality);*

(2) For many (motion) systems $\mathcal{G}_{eu}(j\omega) \to 0$ for $|\omega| \to \infty$, resulting in condition (11) *being satisfied automatically;*

(3) The frequency-domain circle-criterion condition (12) *can be verified graphically in a Nyquist diagram using (measured) frequency response data. We care to stress that this represents the power of the conditions in Theorem 6 in terms of practical applicability, which will be illustrated using an industrial case study in Section 4.*

Note that under the hypothesis of the theorem, the closed-loop reset control system is pre-ISS and the values of (A_r, B_r, C_r) as in (1) *will only affect the performance.*

Remark 8 *Note that our conditions are not limited to control configurations as depicted in Fig. 1. Consider, for instance, the configuration as in Fig. 3, which is commonly used in the literature, see, e.g., [1, 4, 20, 29]. In such a case, the conditions of Theorem 6 still apply for $\mathcal{G}_{eu}(s) = \mathcal{P}(s)\mathcal{C}(s)$.*

4 Case-study on an industrial piezo-actuated motion system

In this section, we demonstrate the effectiveness of our newly proposed stability conditions by considering an industrial case study of the control of the z-axis of a piezo-actuated motion system that is used in the lithography industry.

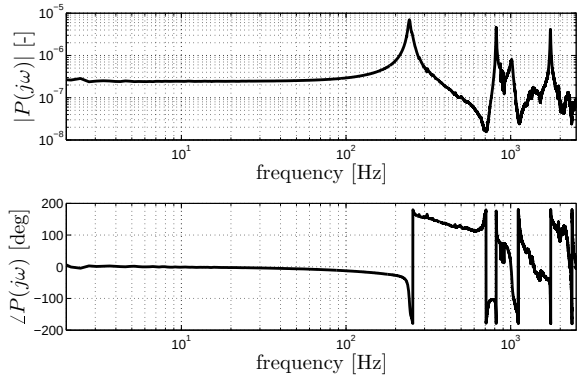

Fig. 4. Measured frequency response function of the lens system in z-direction.

4.1 Problem setting

During the process of wafer scanning, light from an (extreme) ultra-violate source travels through an optical path, see, e.g., [7]. This optical path includes a reticle, containing a blueprint of the integrated circuits to be processed, and a lens system. The lens system consists of several lens elements that are individually controlled by piezo actuators during the scanning process. Due to the limited stroke of the piezo actuators, a calibration, or so-called 'shuffle motion', needs to be performed whenever stroke limitations occur (which may happen more than once during a full wafer exposure). The duration of such a shuffle motion should be kept as small as possible because it compromises machine throughput, i.e., the amount of wafers that can be processed per unit of time is decreased because the scanning process is interrupted during a shuffle motion. Moreover, also from a control point-of-view the occurrence of a shuffle motion poses potential problems. Namely, during a shuffle motion the piezo-actuated system operates in an open-loop mode such that after the shuffle, i.e., when closing the loop again, the motion system (which then operates in scanning mode) suffers from an initial value problem. This problem becomes even more pronounced in view of the disturbance rejection properties required during scanning mode, for which a proportional (double) integral controller (PI^2D), i.e., a controller with two integrators, is preferred over PID control with one integrator, while (additional) integral action deteriorates the transient performance to errors induced by the shuffle motion.

4.2 Controller design

In this section, we will design a reset controller of the form (1), (2), which consists of an LTI controller with

integral action combined with an additional Clegg integrator. The motivation for such a reset controller stems from the problem setting, i.e., due to the double integral action it is expected that good disturbance attenuation properties are maintained during a scanning motion, while the transient behavior is expected to be improved compared to a PI^{2}D controller because one of the two integrators is allowed to reset its buffer. In order to compare the obtained results, also two LTI controllers are designed, namely, a PID and a PI^{2}D controller. All three controllers can be implemented in the control architecture as in Fig. 1, while the design process (of all three considered controllers) will be entirely based on measured frequency-domain data. Here we want to emphasize that the new perspective on reset control systems as presented in this paper allows for such favorable design properties for reset controllers.

Consider Fig. 4, which depicts the measured frequency response function (FRF) of the plant $\mathcal{P}(j\omega)$, $\omega \in \mathbb{R}$. Based on this plant FRF, the nominal controller $\mathcal{C}(s)$, $s \in \mathbb{C}$, of Fig. 1 is designed using classical loop-shaping techniques, see, e.g., [24, 26], and is given by

$$\mathcal{C}(s) = \mathcal{C}_{pid}(s)\mathcal{C}_{n,1}(s)\mathcal{C}_{n,2}(s)\mathcal{C}_{lp}(s), \qquad (31)$$

which consists of a series connection of a PID controller $\mathcal{C}_{pid}(s)$, two notch filters $\mathcal{C}_{n,i}(s)$, $i = 1, 2$, and a second-order low-pass filter $\mathcal{C}_{lp}(s)$. We consider the following three controllers:

(1) An LTI PID-type controller $\mathcal{C}_{\text{PID}}(s) := \mathcal{C}(s)$, with $\mathcal{C}(s)$ as in (31). This results in the control architecture as in Fig. 1 in which $\mathcal{R}$ is absent;
(2) An LTI PI^{2}D-type controller $\mathcal{C}_{\text{PI}^2\text{D}}(s) := \mathcal{C}_i(s)\mathcal{C}(s)$, with $\mathcal{C}(s)$ as in (31) designed in series with an additional lag filter

$$\mathcal{C}_i(s) = \frac{s + \omega_i}{s} = \frac{\omega_i}{s} + 1, \qquad (32)$$

in which $\omega_i \in \mathbb{R}_{>0}$ denotes the integrator cut-off frequency. This results in the control architecture as in Fig. 1 in which $\mathcal{R} = \frac{\omega_i}{s}$ (and thus represents an LTI integrator without any reset action);
(3) A reset controller $\mathcal{C}_{\mathcal{R}}$. In its basis, this controller is similar to the $\mathcal{C}_{\text{PI}^2\text{D}}(s)$ controller (thus with the same $\omega_i \in \mathbb{R}_{>0}$ and $\mathcal{C}(s)$ as in (31)), with the essential difference that $\mathcal{R}$ is not LTI but represents a *Clegg integrator*. This yields the control architecture as in Fig. 1 with $\mathcal{R}$ given by (1), (2), in which $\alpha \in (0, \infty)$ is yet to be determined and $(A_r, B_r, C_r) = (0, \omega_i, 1)$, see, e.g., (3).

Closed-loop stability using both LTI controllers, i.e., the $\mathcal{C}_{\text{PID}}(s)$ and $\mathcal{C}_{\text{PI}^2\text{D}}(s)$ controller, can be verified using standard linear arguments, e.g., using the Nyquist stability criterion, see [24]. Here, we will only discuss how our newly proposed conditions in Theorem 6 can help

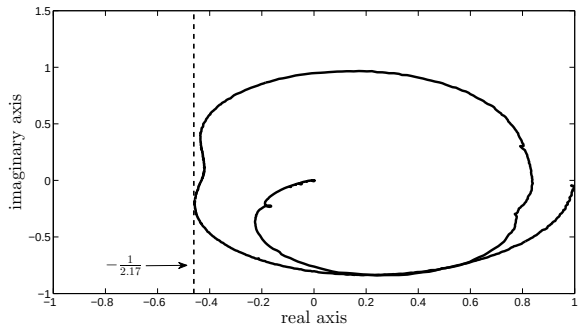

Fig. 5. Nyquist diagram of $\mathcal{G}_{eu}(j\omega)$ showing that the circle criterion condition $Re(\mathcal{G}_{eu}(j\omega)) > -\frac{1}{\alpha}$, is met for all $\omega \in \mathbb{R}$ with $\alpha = 2.17$.

in assessing closed-loop stability for the controller $\mathcal{C}_{\mathcal{R}}$. These conditions are verified as follows: the satisfaction of Assumption 2 is rather trivial, since the Clegg integrator is a one-dimensional system. Condition (I) will be satisfied by design of a stabilizing feedback controller $\mathcal{C}(s)$ as in (31), see also Remark 7. The first requirement of condition (II), i.e., (11), is satisfied as $\mathcal{G}_{eu}(j\omega) \to 0$ for $\omega \to \infty$. Finally, the circle criterion condition (12), which is verified by means of the Nyquist diagram of $\mathcal{G}_{eu}(j\omega)$ in Fig. 5. This figure shows that $Re(\mathcal{G}_{eu}(j\omega)) > -\frac{1}{\alpha}$, for $\alpha \in (0, 2.17]$ is met for all $\omega \in \mathbb{R}$. In the remainder of this case study, we take $\alpha = 2.17$ resulting that the input/output pair $(e, -u)$ of $\mathcal{R}$ as in (1), (2) is confined to the sector $[0, 2.17]$.

4.3 Experimental verification

In this section, we present experimental results in the form of the moving average (MA) filtered error response [1], which is defined as

$$\text{MA} := \frac{1}{T_e} \int_{-\frac{T_e}{2}}^{\frac{T_e}{2}} e(t)dt, \qquad (33)$$

in which T_e represents the exposure time, and $e(t)$ represents the position error of the z-axis as a function of time t.

Consider Figs. 6 and 7 in which the measurement results are depicted during scanning motion and shuffle motion, respectively. Both figures show the MA filtered error responses for four different controller configurations, namely: $\mathcal{C}_{\text{PID}}(s)$, $\mathcal{C}_{\text{PI}^2\text{D}}(s)$, and $\mathcal{C}_{\mathcal{R}}$ with $\alpha \in \{2.17, \infty\}$. Fig. 8 depicts the control signals for the four controller configurations after a shuffle motion. This figure demonstrates the ability of the reset integrators to reset their

[1] The use of MA filtered error responses is common practice in the lithography industry, see, e.g., [7]. Note, however, that the actual time instances of resets are not immediately detectable from these *filtered* error responses.

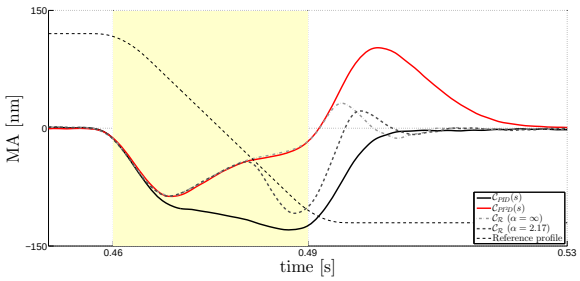

Fig. 6. Moving average (MA) filtered error responses during a scanning motion under different controller configurations.

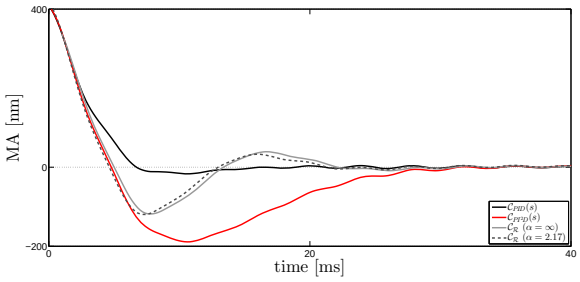

Fig. 7. Moving average (MA) filtered error responses during a shuffle motion under different controller configurations.

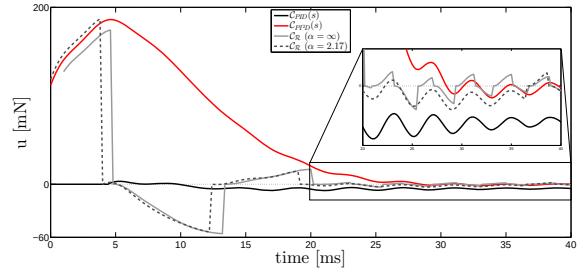

Fig. 8. Control signals after a shuffle motion under different controller configurations.

buffer whenever $eu \geq -\frac{1}{\alpha}u^2$, thereby allowing to enhance the transient performance. Moreover, note that for the considered trajectories the reset times are indeed far apart and Zeno behaviour is not appearing. Hence, the pre-ISS results indeed apply to these t-complete solutions (see also Remark 5).

Let us now focus on the resulting error responses using both linear controllers. During scanning motion $\mathcal{C}_{\mathrm{PI^2D}}(s)$ clearly shows favorable disturbance rejection properties as the resulting MA filtered error response is much smaller during the evaluation window (this window is directly linked to the exposure of one exposure area on the wafer [7], and is indicated by the yellow surface in Fig. 6). However, during a shuffle motion, the $\mathcal{C}_{\mathrm{PI^2D}}(s)$ controller induces significantly more overshoot and a larger settling time compared to the $\mathcal{C}_{\mathrm{PID}}(s)$ controller, as depicted in Fig. 7.

These results are typical for one of the most well-known linear control design trade-offs, i.e., adding integral action to a feedback control system improves the disturbance rejection properties at a cost of a decrease in transient performance (in terms of an increase in overshoot and settling time), see, e.g., [23]. By considering $\mathcal{C}_{\mathcal{R}}$ instead, and hence, allowing one of the integrators to reset its buffer (see Fig. 8) whenever $eu \geq -\frac{1}{\alpha}u^2$, we aim to achieve 'the best of both worlds', i.e., maintaining the disturbance rejection properties associated with a double integrator, while the transient response is comparable to a controller with a single integrator. Consider therefore again Figs. 6 and 7. These figures reveal that $\mathcal{C}_{\mathcal{R}}$ with $\alpha = \infty$ results in comparable disturbance rejection properties as $\mathcal{C}_{\mathrm{PI^2D}}(s)$, while its overshoot and settling behavior is much better. However, closed-loop stability is only guaranteed for all $\alpha \in (0, 2.17]$, based on the sufficient conditions in Theorem 6. So let us focus on the MA filtered error responses of $\mathcal{C}_{\mathcal{R}}$ with $\alpha = 2.17$. Fig. 7 shows that the overshoot and settling is comparable to $\mathcal{C}_{\mathcal{R}}$ with $\alpha = \infty$, but its disturbance rejection properties are worse. This can be explained by the fact that a smaller value of α typically leads to the reset controller resetting its buffer sooner, see Fig. 8, while this buffer (integral action) is actually necessary to suppress the effect of the disturbance. Nevertheless, the disturbance rejection properties are still considerably better compared to the $\mathcal{C}_{\mathrm{PID}}(s)$ controller, while the control signals of both reset controllers show that the time between two consecutive resets is larger than the sampling time of $2 \cdot 10^{-4}$ s) and no Zeno event occurs.

5 Conclusions

In this paper, we presented novel conditions for the stability of reset control systems that can be verified based on (measured) frequency response data of the linear part of the closed-loop system. As the stability conditions are based easy-to-obtain frequency response data, and hence, without the necessity of an (accurate) parametric system model and numerically solving LMIs, they interface well with the current industrial (motion) control design practice. We illustrated this also via experimental results on an industrial piezo-actuated motion system. As such, these new results may contribute to the (further) industrial acceptance of reset controllers, which in itself provide great opportunities in increasing the performance of many linear (motion) systems.

A Hybrid system notation

According to [12], solutions of (9), (2) are defined on hybrid time domains. A *compact hybrid time domain* is a set $E = \bigcup_{j=0}^{J-1}[t_j, t_{j+1}] \times \{j\} \subset \mathbb{R}_{\geq 0} \times \mathbb{N}$ with $J \in \mathbb{N}_{>0}$ and $0 = t_0 \leq t_1 \leq \cdots \leq t_J$. A *hybrid time domain* is a set $E \subset \mathbb{R}_{\geq 0} \times \mathbb{N}$ such that $E \cap ([0, T] \times \{0, 1, \ldots, J\})$ is a compact hybrid time domain for each $(T, J) \in E$. A

hybrid signal is a function defined on a hybrid time domain. A hybrid signal $w : \operatorname{dom} w \to \mathbb{R}^{n_w}$ is a *hybrid input* if $w(\cdot, j)$ is Lebesgue measurable and locally essentially bounded for each j. We write for a hybrid input signal that $w \in \mathcal{L}_\infty$ if $\|w\|_\infty := \operatorname{ess\,sup}_{(t,j)\in\operatorname{dom} w} \|w(t,j)\| < \infty$. A hybrid signal $x : \operatorname{dom} x \to \mathbb{R}^{n_x}$ is a *hybrid arc* if $x(\cdot, j)$ is locally absolutely continuous for each j.

A hybrid arc $x : \operatorname{dom} x \to \mathbb{R}^{n_x}$ and a hybrid input $w : \operatorname{dom} w \to \mathbb{R}^{n_w}$ form a *solution pair* (x, w) to (9), (2) if $\operatorname{dom} x = \operatorname{dom} w$, $(e(0,0), -u(0,0)) \in \mathcal{F} \cup \mathcal{J}$, and

(1) for all $j \in \mathbb{N}$ and almost all $(t, j) \in \operatorname{dom} x$

$$\dot{x}(t,j) = \bar{A}x(t,j) + \bar{B}w(t,j), \text{ and } (x(t,j), w(t,j)) \in \tilde{\mathcal{F}}$$

(2) for all $(t, j) \in \operatorname{dom} x$ such that $(t, j+1) \in \operatorname{dom} x$

$$x(t,j+1) = \bar{A}_r x(t,j), \text{ and } (x(t,j), w(t,j)) \in \tilde{\mathcal{J}}$$

with $\tilde{\mathcal{F}} := \{(x,w) \in \mathbb{R}^{n_x} \times \mathbb{R}^{n_w} \,|\, (e,-u) \in \mathcal{F}\}$ and $\tilde{\mathcal{J}} := \{(x,w) \in \mathbb{R}^{n_x} \times \mathbb{R}^{n_w} \,|\, (e,-u) \in \mathcal{J}\}$.

References

[1] W.H.T.M. Aangenent, G. Witvoet, W.P.M.H. Heemels, M.J.G. van de Molengraft, and M. Steinbuch. Performance analysis of reset control systems. *Int. J. of Robust and Nonlinear Control*, 20(11):1213–1233, 2010.

[2] A. Baños and A. Barreiro. *Reset Control Systems*. Springer, 2012.

[3] A. Baños, J.I. Mulero, A. Barreiro, and M.A. Davó. An impulsive dynamical systems framework for reset control systems. *Int. J. of Control*, pages 1–23, 2016. Article in Press.

[4] O. Beker, C. V. Hollot, Y. Chait, and H. Han. Fundamental properties of reset control systems. *Automatica*, 40(6):905–915, 2004.

[5] O. Beker, C.V. Hollot, and Y. Chait. Plant with integrator: An example of reset control overcoming limitations of linear feedback. *IEEE Trans. Autom. Control*, 46(11):1797–1799, 2001.

[6] O. Beker, C.V. Hollot, Q. Chen, and Y. Chait. Stability of a reset control system under constant inputs. In *Proc. of the American Contr. Conf.*, volume 5, pages 3044–3045, 1999.

[7] H. Butler. Position control in lithographic equipment. *Contr. Syst. Mag.*, 31(5):28–47, 2011.

[8] C. Cai and A.R. Teel. Characterizations of input-to-state stability for hybrid systems. *Syst. and Contr. Letters*, 58(1):47–53, 2009.

[9] J. Carrasco, A. Baños, and A. van der Schaft. A passivity-based approach to reset control systems stability. *Syst. and Contr. Letters*, 59(1):18–24, 2010.

[10] J. Clegg. A nonlinear integrator for servomechanisms. *Trans. of the A.I.E.E.*, 77(Part-II):41–42, 1958.

[11] F. Forni, D. Nešić, and L. Zaccarian. Reset passivation of nonlinear controllers via a suitable time-regular reset map. *Automatica*, 47(9):2099–2106, 2011.

[12] R. Goebel, R.G. Sanfelice, and A.R. Teel. *Hybrid dynamical systems: modeling, stability and robustness*. Princeton University Press, 2012.

[13] M.F. Heertjes, K.G.J. Gruntjens, S.J.L.M. van Loon, N. Kontaras, and W.P.M.H. Heemels. Design of a variable gain integrator with reset. In *Proc. of the American Contr. Conf.*, pages 2155–2160, 2015.

[14] M.F. Heertjes and M. Steinbuch. Stability and performance of a variable gain controller with application to a dvd storage drive. *Automatica*, 40(4):591–602, 2004.

[15] J.P. Hespanha. *Linear systems theory*. Princeton University Press, 2009.

[16] I. Horowitz and P. Rosenbaum. Nonlinear design for cost of feedback reduction in systems with large parameter uncertainty. *Int. J. of Control*, 21(6):977–1001, 1975.

[17] B.G.B. Hunnekens, N. van de Wouw, M.F. Heertjes, and H. Nijmeijer. Synthesis of variable gain integral controllers for linear motion systems. *IEEE Trans. Contr. Syst. Technology*, 23(1):139–149, 2015.

[18] H.K. Khalil. *Nonlinear Systems*. Prentice Hall, 2000.

[19] D. Nešić, A.R. Teel, and L. Zaccarian. Stability and performance of SISO control systems with first-order reset elements. *IEEE Trans. Autom. Control*, 56(11):2567–2582, 2011.

[20] D. Nešić, L. Zaccarian, and A.R. Teel. Stability properties of reset systems. *Automatica*, 44(8):2019–2026, 2008.

[21] F.S. Panni, H. Waschl, D. Alberer, and L. Zaccarian. Position regulation of an EGR valve using reset control with adaptive feedforward. *IEEE Trans. Contr. Syst. Technology*, 22(6):2424–2431, 2014.

[22] C. Prieur, S. Tarbouriech, and L. Zaccarian. Lyapunov-based hybrid loops for stability and performance of continuous-time control systems. *Automatica*, 49(2):577–584, 2013.

[23] M.M. Seron, J.H. Braslavsky, and G.C. Goodwin. *Fundamental Limitations in Filtering and Control*. Berlin: Springer, 1997.

[24] S. Skogestad and I. Postlethwaite. *Multivariable Feedback Control: Analysis and Design*. John Wiley & sons, Ltd, 2005.

[25] E. D. Sontag and Y. Wang. On characterizations of the input-to-state stability property. *Syst. Contr. Lett.*, 24(5):351–359, 1995.

[26] M. Steinbuch and M.L. Norg. Advanced motion control: An industrial perspective. *European J. of Control*, 4(4):278–293, 1998.

[27] N. van de Wouw, H.A. Pastink, M.F. Heertjes, A.V. Pavlov, and H. Nijmeijer. Performance of convergence-based variable-gain control of optical storage drives. *Automatica*, 44(1):15–27, 2008.

[28] L. Zaccarian, D. Nešić, and A.R. Teel. First order reset elements and the clegg integrator revisited. In *Proc. of the American Contr. Conf.*, volume 1, pages 563–568, 2005.

[29] L. Zaccarian, D. Nešić, and A.R. Teel. Analytical and numerical Lyapunov functions for SISO linear control systems with first-order reset elements. *Int. J. of Robust and Nonlinear Control*, 21(10):1134–1158, 2011.

[30] G. Zhao and J. Wang. On $\mathcal{L}$-gain performance improvement of linear systems with Lyapunov-based reset control. *Nonlinear Analysis: Hybrid Systems*, 21:105 – 117, 2016.

[31] Y. Zheng, Y. Chait, C.V. Hollot, M. Steinbuch, and M. Norg. Experimental demonstration of reset control design. *Contr. Eng. Practice*, 8(2):113–120, 2000.